İSTANBUL UNIVERSITY CERRAHPAŞA

ORIGINAL ARTICLE
Electrica 2025; 25: 1-16

Advanced Power Quality Enhancement and Harmonic Filtering in Solar Photovoltaic Integrated Cascaded H-Bridge Inverters

Vijay S. Pawar, Prashant J. Gaidhane

Department of Electrical Engineering, Government College of Engineering Jalgaon, Jalgaon, Maharashtra, India

Cite this article as: V. S. Pawar and P. J. Gaidhane, "Advanced power quality enhancement and harmonic filtering in solar photovoltaic integrated cascaded H-bridge inverters," *Electrica*, 25, 0210, 2025. doi: 10.5152/electrica.2025.24210.

WHAT IS ALREADY KNOWN ON THIS TOPIC?

- *Cascaded H-Bridge (CHB) multilevel inverters are well-established in improving output waveform quality and reducing Total Harmonic Distortion (THD) in grid-connected PV systems.*
- *Deep learning models, especially LSTM and its variants, have been increasingly applied to optimize PV system performance, including power output forecasting and fault detection.*
- *Bio-inspired and evolutionary optimization algorithms (e.g., PSO, GA) are commonly used to enhance the tuning of controllers and improve learning efficiency in power system applications.*

WHAT THIS STUDY ADDS ON THIS TOPIC?

- *Introduces a novel combination of a bidirectional Long Short-Term Memory (BiLSTM) network with the Puma*

Corresponding author:
Vijay S Pawar

E-mail:
vijayspawarvsp@gmail.com

Received: December 19, 2024
Revision Requested: February 25, 2025
Last Revision Received: March 14, 2025
Accepted: March 31, 2025
Publication Date: July 11, 2025

DOI: 10.5152/electrica.2025.24210

ABSTRACT

Globally, grid-connected solar power systems are growing in popularity, but a significant challenge is optimizing output power while preserving excellent power quality. The depletion of fossil resources and the environmental issues surrounding traditional energy sources have led to a surge in interest in renewable energy, especially solar energy. This research suggests a hybrid control technique for enhancing the power quality of solar photovoltaic systems that are grid-connected by mitigating the effect of harmonic currents on system performance, even when linear loads are involved. The technique makes use of a 17-level cascaded H-bridge multilevel inverter that is coupled with the Puma optimizer, a bidirectional long short-term memory (BiLSTM) network, and an advanced multi-head cross-attention-based optimizer. The Puma optimizer enhances the deep learning network's learning process, while the BiLSTM network regulates the input to the cascaded H-bridge multilevel inverter to drive its output. This combination improves the efficiency of the photovoltaic generator and maximizes power extraction in the system. Simulations are performed in MATLAB to improve power quality and filter harmonics in solar photovoltaic systems for two cases: linear loads with and without fault conditions, with a constant level of radiation at 1000 W/m^2. The fundamental frequency of the 17-level cascaded H-bridge multilevel inverter is 50 Hz, with a magnitude of approximately 397.8. The overall harmonic distortion is kept at 3.96%. Additionally, the Puma optimizer has the lowest mean squared error (0.025).

Index Terms—multilevel inverter, PV power systems, harmonic distortion reduction, harmonic filtering, power quality

I. INTRODUCTION

Power quality in Photovoltaic (PV) systems is increasingly crucial in modern electrical design. Beyond meeting energy demands, the emphasis is now on ensuring a reliable and flexible power supply. Problems such as line faults, harmonics, and voltage fluctuations pose challenges to engineers in enhancing system efficiency and reliability while incorporating renewable energy sources [1-2]. Fossil fuels' negative environmental effects, like pollution and greenhouse gas emissions, have prompted a shift to renewable energy sources (RES), like solar, wind, and biogas, as more ecologically acceptable substitutes. Among these, PV has become the most prevalent RES due to its inexhaustible, pollution-free, and environmentally friendly nature, with expectations of substantial energy production in the coming decades [2]. PV systems generate DC electricity, necessitating integration into existing AC systems via converters [3-4]. Numerous electronic converters have been developed, with Multilevel Inverters (MLI) emerging as particularly effective for AC applications. MLI provides several benefits over traditional converters, including superior power quality waveforms, higher voltage handling capabilities, and reduced switching losses [5].

Efficient use of solar energy entails the deployment of MPPT (maximum power point tracking) systems, which are critical in maximizing PV system performance by continually varying the operating points to provide maximum power output [6]. Several methods have been investigated in the literature for achieving this purpose. Perturb and Observe (P&O) is the technique that repeatedly varies the voltage and detects the resulting power variation to locate the maximum power point [7]. The incremental conductance method enhances P&O by using the power

optimizer and multi-head cross attention mechanism, enhancing the learning precision and dynamic control of the inverter system. v Implements a 17-level cascaded H-bridge inverter, which is more complex than conventional multilevel inverters, offering finer voltage steps and superior harmonic filtering capabilities.

- *Implements a 17-level cascaded H-bridge inverter, which is more complex than conventional multilevel inverters, offering finer voltage steps and superior harmonic filtering capabilities. v Unlike many studies focusing only on ideal conditions, this research evaluates power quality improvement under both normal and fault scenarios, proving its robustness and real-world applicability.*
- *Unlike many studies focusing only on ideal conditions, this research evaluates power quality improvement under both normal and fault scenarios, proving its robustness and real-world applicability. v Achieves a significant reduction in Total Harmonic Distortion (THD) to 3.96%, along with a low mean squared error of 0.025 demonstrating improved accuracy in system response and control. The proposed system effectively maximizes power extraction from the PV generator even under challenging load conditions, contributing to higher overall system efficiency.*

derivative with respect to voltage to determine the direction of the maximum power point, leading to quicker convergence and fewer oscillations around the peak power point [8]. Although the above techniques are relatively simple and easy to implement, their accuracy is compromised under varying environmental conditions [9]. Fuzzy Logic Control (FLC) leverages fuzzy logic to address the uncertainty and non-linearity present in PV systems, resulting in robust performance across various conditions. Artificial Neural Networks (ANN) employ historical data to learn and predict the maximum power point, providing high accuracy and adaptability [10]. In earlier research, conventional control techniques like PI and fuzzy logic controllers had difficulty adapting to dynamic variations of loads as well as faults. Moreover, conventional optimization algorithms like PSO and GA lacked efficiency while coping with the highly complex search spaces of realistic high-dimensional engineering applications, hence causing suboptimal harmonic filtering efficiency. Hybrid MPPT methods combine the strengths of different techniques to achieve more reliable and efficient performance. These methods are dynamically adapted to changing conditions, ensuring the PV system operates close to its maximum potential.

A. Related Work and Motivation

The literature review examines the advancements in power quality enhancement for solar PV systems through the use of various controllers and power electronic devices, as discussed in references [11-20].

Rajesh et al. [11] presented a Cascaded Multilevel Inverter (CMLI) to enhance control pulses and ensure high Power Quality (PQ) while maximizing PV energy. The optimization approach generates control signals, with a Recurrent Echo State Neural Network (RERNN) used to produce real-time control signals for the CMLI.

Yadav et al. [12] introduced an improved multicarrier modulation technique for single-source PV-based CHBMLI. The new modulation scheme was a combination of pulse and triangular carrier functions, referred to as the Modified Level Arranged Carrier Scheme (MLACS). In MLACS, the frequency of the pulse function was multiplied by the carrier wave.

Anusha et al. [13] introduced a novel 15-level CMLI tailored for renewable energy applications, integrating PV systems and batteries. The innovative control strategy ensures optimized performance across diverse operational conditions.

Chamarthi et al. [14] presented two advanced Pulse Width Modulation (PWM) methods designed for Five-Level Neutral Point Clamped H-Bridge Configurations (FLNPCHC), which were further cascaded to form MLI.

Jain et al. [15] presented a strong method of enhancing PQ and guaranteeing the reliable functioning of two-stage solar photovoltaic grid-connected systems under fluctuating circumstances. The model utilized a hybrid Phase-Locked Loop (PLL) for synchronization purposes. Furthermore, DC link voltage sliding mode controllers and circularly integral class-sliding mode current regulators were considered, as well as monitored the grid currents accurately.

Prasad et al. [16] introduced a pioneering method employing the HGSR (Hybrid Group Search Integrated Rider)-MPPT to maximize PV integration into the grid. The SARC (Self-Adaptive Rao Control) method enabled the generation of switching pulses for the converter.

Das et al. [17] presented a novel Modified Pack U-Cell (MPUC) MLI configuration tailored for smart grid applications. The control strategy utilizes instantaneous active and reactive current methods to produce reference currents, in addition to an Adaptive Fuzzy Hysteresis Current Controller (AFHCC) to control switching signals with high accuracy.

Mohanty et al. [18] developed a reduced switch MLI through the use of Black Widow Optimization (BWO), a bio-inspired metaheuristic algorithm. The BWO algorithm showed superior efficiency in minimizing Total Harmonic Distortion (THD) within short periods. Furthermore, its convergence speed and accuracy were compared with those of two other bio-inspired algorithms. The design was mainly focused on the configuration of a 13-level MLI using a single PV source that was made for grid integration purposes without any interruptions.

Govind et al. [19] introduced a systematic method to enhance PQ utilizing SAPF (Shunt Active Power Filter). The study integrates neural network techniques to optimize SAPF switching control under unbalanced conditions.

Bansal et al. [20] recommended an inventive technique for improving the operation framework of a single-phase SAPF by combining it with 5-level cascaded MLI and PV array. This technique includes extracting the base part of the load current and effectively managing grid disturbances such as DC offset, phase shift, and harmonic distortions.

B. Problems Identified

There is a critical need for the research due to several key reasons such as grid stability, Harmonic Distortion Reduction, and reduced Energy Losses. Challenges include enhancing control pulses while maximizing energy output and improving harmonic levels in single-source PV-based CHBMLI systems. Optimizing 15-level CMLI for renewable energy applications, especially in integrating PV systems and batteries under varying conditions, is essential. Advanced PWM methods are necessary for better PQ and efficiency in five-level NPC H-bridge configurations, while addressing issues like DC offset and harmonics in two-stage PV grid-tied systems.

C. Novelty and Organization

The study suggests a hybrid control strategy that includes an Evolved Multihead Cross Attention-based Optimizer with a BiLSTM Network (EMCAOBN) and the Puma Optimizer (PO) to enhance the performance of PV systems by managing MPPT, DC-link voltage, and harmonic currents. The complexity is reduced with the minimal-switch CHBMLI structure, dynamic reactive power control, and harmonic filtering for improving grid power quality, thus making the topology viable for solar integration. The following are the objectives:

- Create a hybrid control strategy to improve the power quality of grid-integrated solar photovoltaic systems through efficient filtering of harmonic currents from nonlinear loads.
- Use a BiLSTM network to control the input of a 17-level cascaded H-bridge multilevel inverter to provide the optimal output voltage and minimize harmonic distortion.
- Integrate the Puma optimizer with the developed multi-head cross-attention mechanism to enhance the process of learning, optimize power extraction, and reduce prediction errors during real-time system operation.

The research has the following structure: Section two describes the materials and methods, Section three results and discussion, and Section four conclusion. An overall summary block diagram of the article is given in Fig. 1.

II. MATERIALS AND METHODS

The system includes PV modules, a cascaded multilevel H-bridge inverter, a boost converter, and a grid-interfacing filter. Each string in the PV modules' multi-string structure is coupled to a boost converter to achieve MPPT. According to Kirchhoff's Voltage Law (KVL), the cascaded H-bridge multilevel inverter transforms the PV array's increased DC power into AC voltage, which is then distributed among the output voltage's filter components, grid impedance, and interface inductance. Current injection is controlled by the inverter in accordance with the grid voltage, and energy transfer to the grid is solely current-driven.

The objective is to minimize harmonics and improve power quality for a broader load range, including nonlinear loads. To balance the DC-link capacitor voltage in the proposed inverter, a controller is employed. The controller alters the switching patterns or uses feedback control to regulate capacitor voltages so that the system remains stable and generates proper multilevel output without considering ideal sources. Fig. 1 illustrates the advanced PQ enhancement and harmonic filtering in the solar PV system.

A. Modelling of Solar PV

Various series and parallel arrangements of multiple PV modules are connected to each other in a PV array. This is mathematically expressed in (1):

$$i_m = i_{PH} - i_R\left[\exp\left(\frac{v + r_{se} i_m}{v_t a}\right) - 1\right] - \frac{v + r_{se} i_m}{r_{sh}} \quad (1)$$

where, i_m, i_{PH}, i_R, v, v_t, r_{se}, r_{sh} represents terminal current, the current generated by photons due to incident light, the diode saturation current, terminal voltage, thermal voltage, and resistances in series and parallel, respectively.

B. Cascaded H-bridge Multilevel Inverter

Fig. 2 illustrates a CHBMLI topology designed for three-phase operation. Three phases are connected to a series of H-bridge cells, which consist of switches (S1-S12) and diodes arranged in a configuration to manage the voltage levels. The DC voltage sources (Vdc)

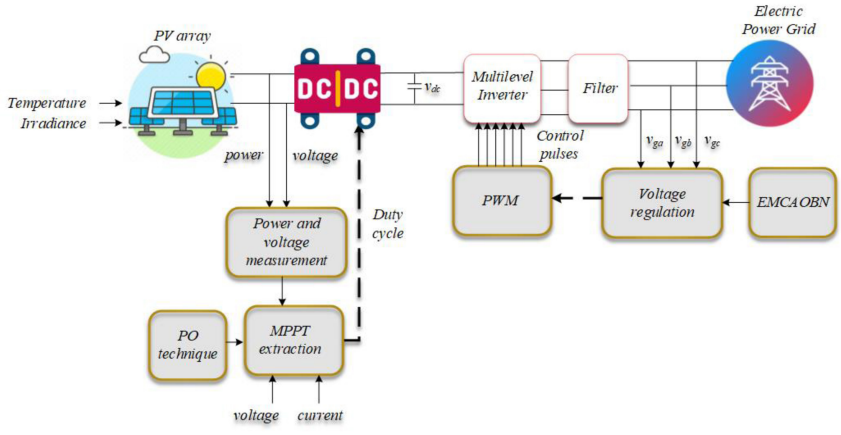

Fig. 1. Advanced PQ enhancement and harmonic filtering in PV.

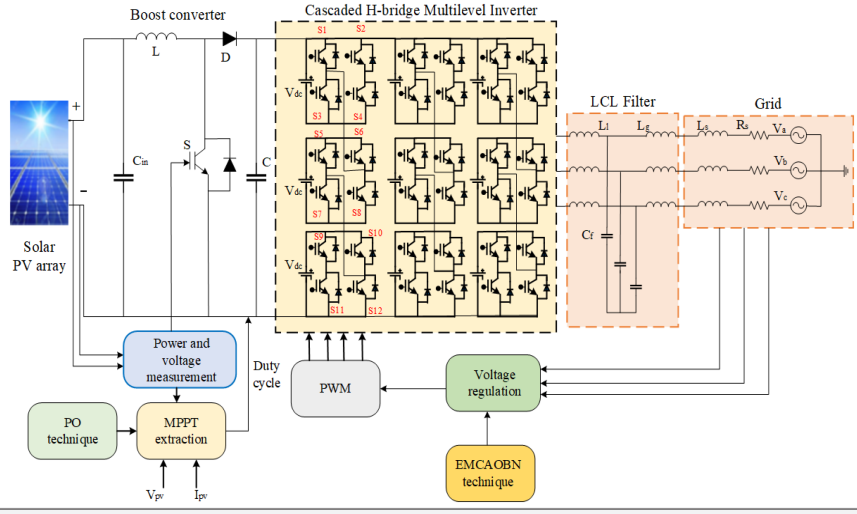

Fig. 2. Cascaded H-bridge multi level inverter.

feed into these H-bridge cells, which modulate the output voltage through the sequential switching of the transistors. The proposed inverter output quality is enhanced by decreasing harmonic distortion in this configuration, which allows the generation of several voltage levels.

Table I outlines the switching logic for a CHBMLI to achieve specific output voltage levels. For each desired voltage level, a specific combination of switches (S1-S12) is turned on. Positive voltage levels (+Vdc to +8Vdc) require different sets of switches compared to negative voltage levels (–Vdc to –8Vdc). Zero voltage output is achieved by a unique combination that balances the positive and negative contributions from the H-bridge cells. The combinational logic of the proposed CHBMLI topology is shown in Table II.

TABLE I. SWITCHING SEQUENCE OF CHBMLI

Switches To Be Activated	Output Voltage Levels
2, 3, 5, 6, 9, 12	+8 Vdc
1, 4, 6, 7, 9, 12	+7 Vdc
1, 2, 6, 7, 9, 12	+6Vdc
2, 3, 6, 7, 9, 12	+5 Vdc
1, 4, 5, 8, 9, 10	+4 Vdc
1, 2, 5, 8, 9, 10	+3 Vdc
2, 3, 5, 8, 9, 10	+2 Vdc
1, 4, 5, 6, 9, 10	+ Vdc
1, 2, 5, 6, 9, 10	0
2, 3, 5, 6, 9, 10	–1 Vdc
1, 4, 6, 7, 9, 10	–2 Vdc
1, 2, 6, 7, 9, 10	–3 Vdc
2, 3, 6, 7, 9, 10	–4Vdc
1, 4, 5, 8, 10, 11	–5Vdc
1, 2, 5, 8, 10, 11	–6 Vdc
2, 3, 5, 8, 10, 11	–7 Vdc
1, 4, 5, 8, 10, 11	–8 Vdc

C. MPPT Control

To optimize PV system performance and address mismatches, PV modules operate at different voltages. As shown in Fig. 3, distributed MPPT regulation in a three-phase inverter happens when each H-bridge module contains an MPPT controller that produces the reference DC-link voltage. This is compared to the actual voltage, with a total voltage controller managing errors to set the reference current. Reactive current is adjusted for compensation as needed.

The PWM method is critical to minimize low-order harmonics in inverters. This is done by switching inverter switches ON and OFF repeatedly within a half cycle and modifying the pulse width to regulate the output voltage. This approach is utilized to regulate switches in the CHBMLI to synchronize the output with grid needs. The MPPT controllers receive the voltage and current signals, compute the power, and adjust the DC-link reference voltage. The PI controller controls i_q to vary the reactive power accordingly, allowing compensation.

TABLE II. COMBINATIONAL LOGIC OF PROPOSED CHBMLI TOPOLOGY

Voltage Level	Switches ON
+3Vdc	S1, S4, S7, S10
+2Vdc	S1, S4, S7, S8
+Vdc	S1, S2, S7, S8
0	S2, S3, S6, S7, S10, S11
–Vdc	S3, S4, S6, S7
–2Vdc	S3, S4, S6, S9
–3Vdc	S3, S6, S9, S12

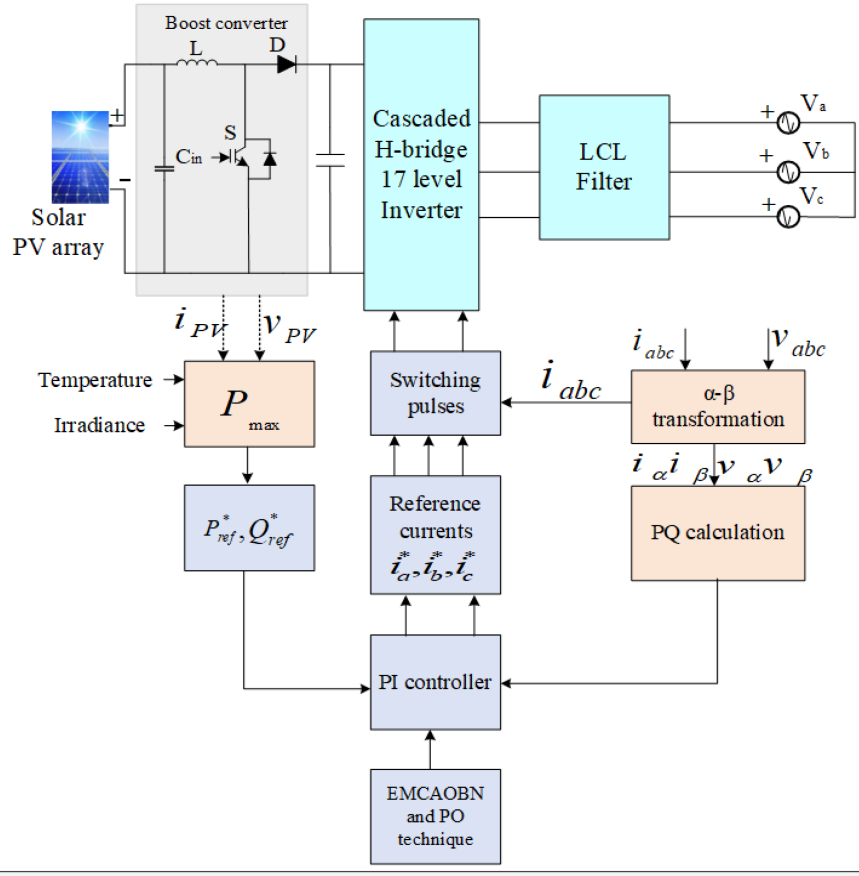

Fig. 3. Control strategy for a CHBMLI.

D. Puma Optimizer for Maximum Power Extraction

Pumas use their intelligence and memory to hunt by revisiting successful locations or exploring new areas [21]. The memory-based nature of the algorithm enables it to revisit good solutions while dynamically venturing into new regions, an advantage, especially in nonlinear, multi-objective optimization problems such as harmonic filtering

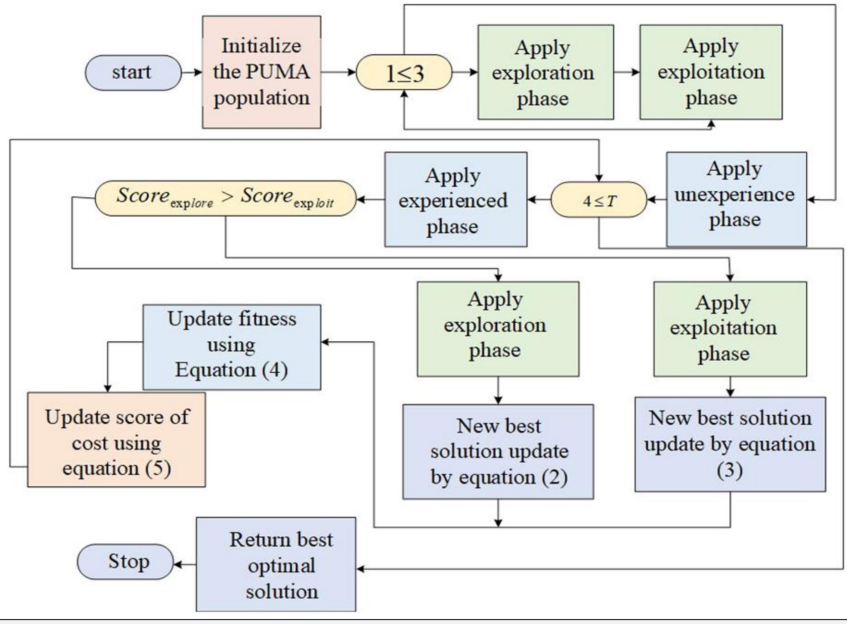

Fig. 4. Flowchart for PO algorithm.

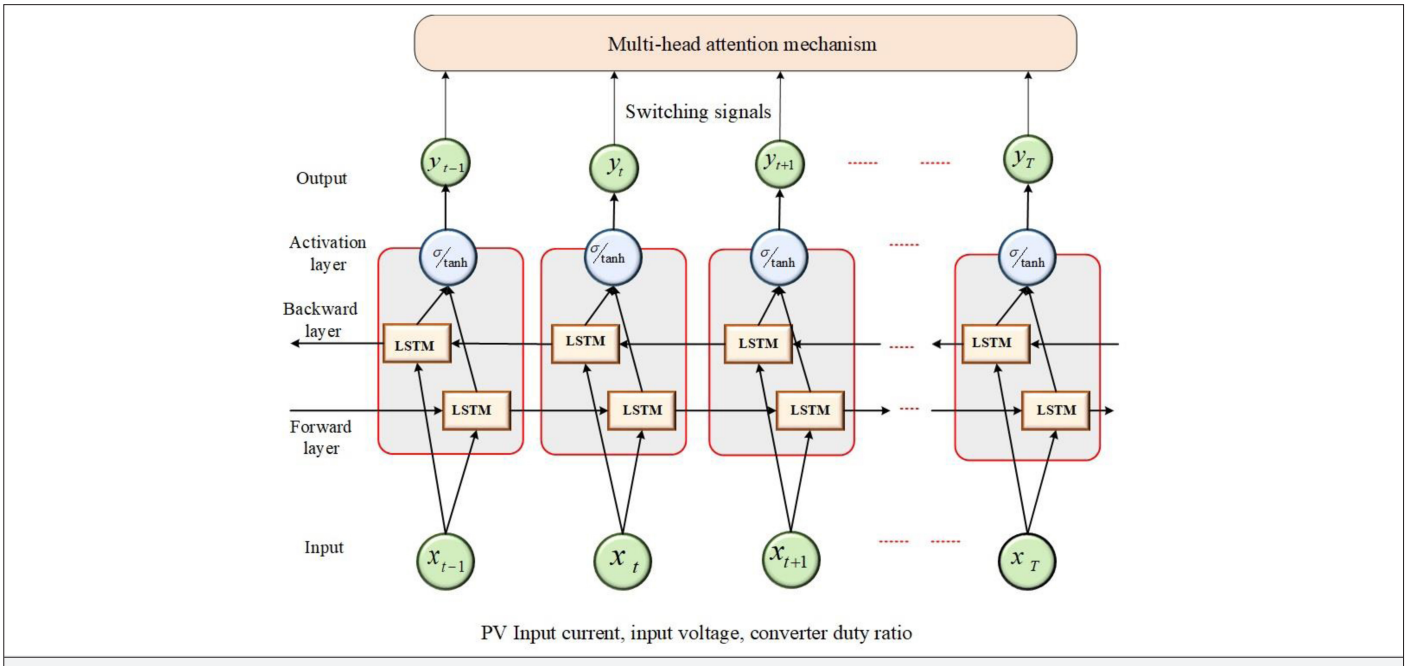

Fig. 5. EMCAOBN with a Bi-LSTM network.

and power quality improvement in photovoltaic systems. PO is more robust and converges faster compared to traditional algorithms in evading local optima. Fig. 4 shows the flowchart for the PO algorithm. Initialize a population of candidate solutions, such as PV input voltage and current. The objective is to maximize PV power, so the fitness function reflects the power output at each candidate voltage.

In the two phases of exploitation and exploration, the experienced puma selects one phase for optimization, with the selection determined by the following (2), (3):

$$f_t^{\text{exploit}} = S_1 \cdot \left| \frac{C_{old}^{\text{exploit}} - C_{new}^{\text{exploit}}}{T_t^{\text{exploit}}} \right| \tag{2}$$

$$f_t^{\text{explore}} = S_1 \cdot \left| \frac{C_{old}^{\text{explore}} - C_{new}^{\text{explore}}}{T_t^{\text{explore}}} \right| \tag{3}$$

where f_t^{explore} and f_t^{exploit} represents the exploration and exploitation phases of the first function are associated with their respective $C_{old}^{\text{exploit}}, C_{new}^{\text{exploit}}$ costs, while the best solutions are represented before and after improvement, corresponding to the costs of the improved best solutions T_t^{explore} over time.

The mathematical selection and upgradation are expressed by the following (4):

$$E_i^{it+1} = \begin{cases} E_i^{old} & f\left(E_i^{new}\right) > f\left(E_i^{old}\right) \text{ and } I < m \\ E_i^{new} & \textit{Otherwise} \end{cases} \tag{4}$$

E. Problem Formulation

Based on the above description, problems are restructured into two distinct objective functions. The objective functions are given in (5), (6):

$$OF_1 = \max\left\{P_{PV}\right\} \tag{5}$$

$$OF_2 = \min\left\{\text{THD}\right\} \tag{6}$$

Where, P_{PV}, THD represents PV output power and THD, respectively.

F. Proposed Based Strategy for Tuning the System Parameters

Multi-head attention mechanism blends the information from many subspaces built by many self-attention layers. It consists of a linear transformation on query ('y'), key ('*e*'), and value ('l'), whereby attention matrix gets worked out via (7) [22-24]:

$$attention(y, e, l) = soft\max\left(\frac{ye^t}{\sqrt{D_f}}\right)l \tag{7}$$

where *softmax*, '*t*', and D_f represents the determinant normalization function, the transpose operation of the matrix, and the scale factor respectively. First, the '*y*', '*e*', and '*l*' parameter matrices are obtained

TABLE III. SOLAR PV ARRAY, 17-LEVEL CASCADED MLI SPECIFICATION

Solar PV Array		**17-Level Cascaded MLI**	
Maximum power	1000W	Capacitor rating	80V, 4700μF
Maximum voltage	290V	Voltage source	400V
Maximum current	345 A	Modulation frequency	50Hz
Open circuit current	368.84 A	Inductive load	98mH
Open circuit voltage	360 V	Load resistance	80 Ω
No of parallel modules	47	Carrier frequency	10 kHz
No of series modules	10	Output voltage, current	400V, 6A

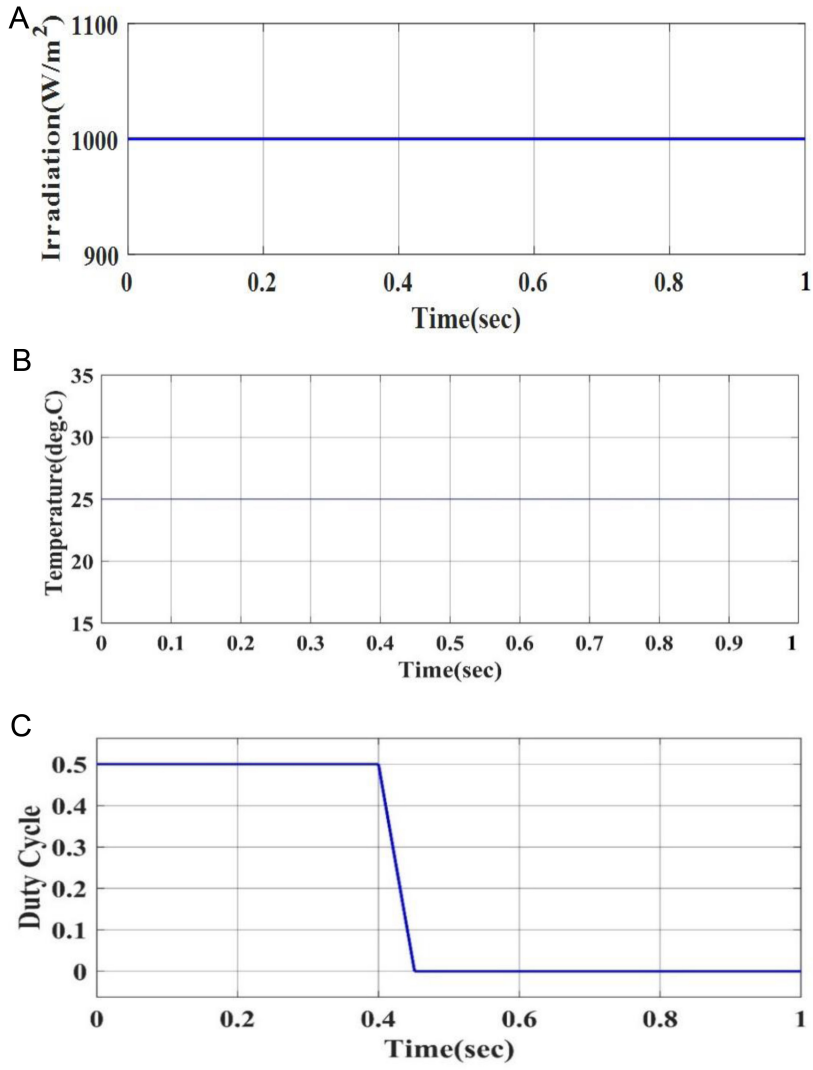

Fig. 6. Analysis of (A) Irradiation, (B) Temperature, and (C) Duty cycle.

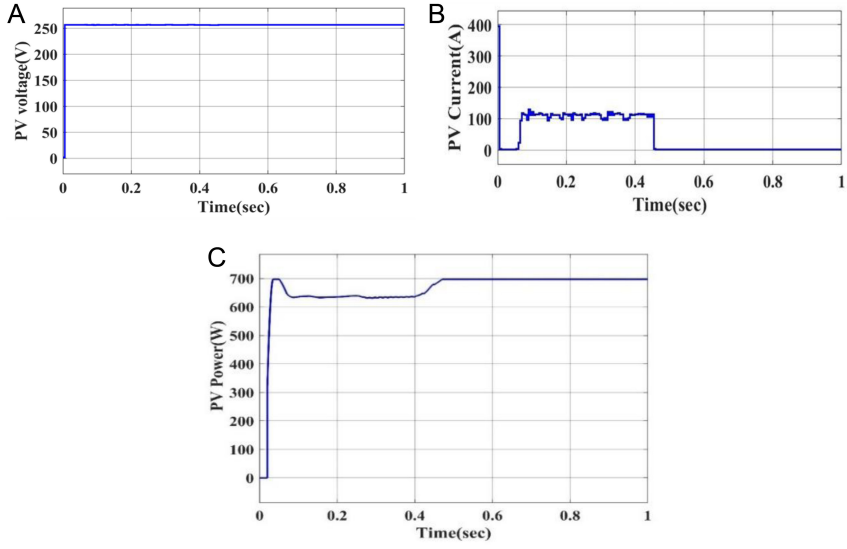

Fig. 7. Response of CHBMLI without fault condition: (a) output current, (b) output voltage, (c) PV voltage, (d) PV current, and (e) PV power.

by multiplying the '*j*' linear transformations in the module. The obtained input 'G' parallels heads to perform different operations.

$$HEAD_j = attention(yv_j^y, ev_j^e, lv_j^l) \quad (8)$$

$$S = MULTIHEAD = (y,e,l) = Concat(HEAD_1 ..... , HEAD_G)v^d \quad (9)$$

where, v_j^y, v_j^e, v_j^l, v^d represents the parameter matrices, '*S*', *Concat*, $HEAD_G$ represents output result, the concatenation operation, and the G^{th} head respectively. In multi-component systems, Bi-LSTM's ability to incorporate bidirectional context offers improved accuracy in characterizing complex interactions and dynamics between diverse materials. Fig. 5 shows the EMCAOBN with a Bi-LSTM Network.

The forget gate vector is given in (10):

$$h_k = \lambda(v_h(y_k) + w_h(g_{k-1}) + B_h \quad (10)$$

In this case, v_h, w_h, B_h indicate weighting matrices.

The cell state vector is given in (11):

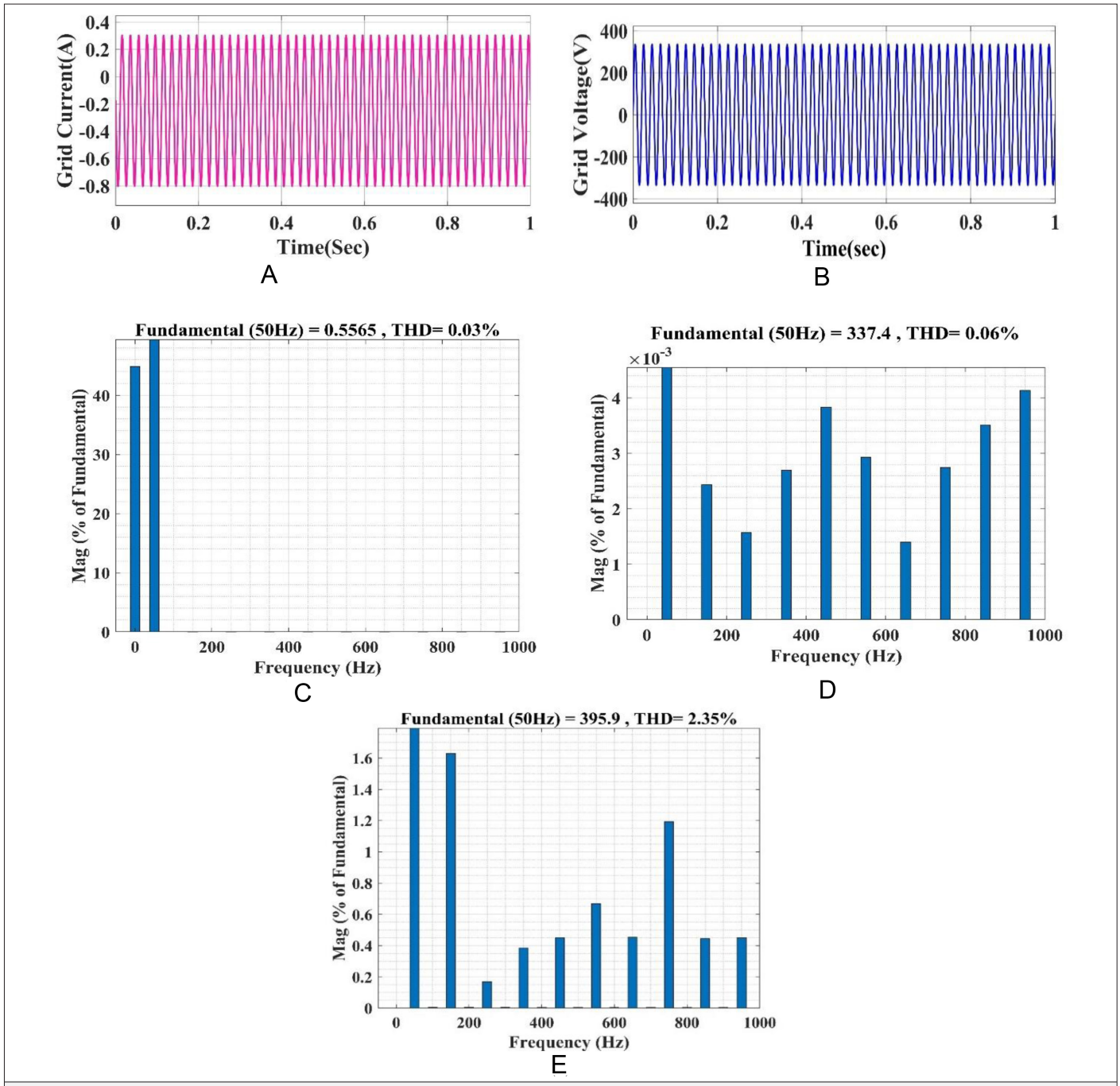

Fig. 8. Analysis of (a) Grid current, (b) Grid voltage, (c) Harmonics of grid current, (d) Harmonics of grid voltage, and (e) THD of 17 level CHBMLI voltage.

$$A_k = (h_k \times A_{k-1}) + I_k \times A'_k \quad (11)$$

where, h_k, A_{k-1} represents forget gate vector and the cell state vector at time step 'k', respectively. The output gate vector (X_k) is given in (12):

$$X_k = \lambda(v_X(y_k) + w_X(g_{k-1}) + B_X \quad (12)$$

Hidden state is given in (13):

$$g_k = (X_k) \times \tan h(A^k) \quad (13)$$

where g_k denotes hidden state. Leverage the output from the multi-head attention mechanism as input features for the Bi-LSTM network to improve its capability in capturing sequential patterns. Apply the PO technique to fine-tune the parameters of the Bi-LSTM and multi-head attention components. Specifically, use the PO exploitation and exploration phases to optimize the attention weights and Bi-LSTM parameters. The EMCAOBN technique, enhances control over the system, particularly for MPPT and managing the CHBMLI output.

III. RESULTS AND DISCUSSIONS

This research introduces the CHBMLI and the EMCAOBN and focuses on the MPPT control for optimizing efficiency in PV systems under constant solar conditions.

The MATLAB simulation results for PQ enhancement and harmonic filtering in PV systems are presented. The delta-connected resistive load is fed by the inverter, in which line and phase voltages are equal in magnitude. In order to reduce voltage and current wave harmonic distortions, an output filter inductor with an inductance value of 4mH/phase is utilized [34]. The specifications are provided in Table III.

Case 1: PV system under linear load without considering fault

Case 2: PV system under linear load with fault

Case 3: PV system under unbalanced and non-linear load with constant irradiation

Case 4: PV system under constant irradiation and non-linear load

A. Case 1

Fig. 6 (a-c) illustrates the variations in PV values for irradiation, temperature, and duty cycle over time. Temperature is maintained at 25 degrees Celsius. The duty cycle remains constant at 0.5 from t = 0 to t = 0.4. After t = 0.4, the duty cycle value slightly decreases and is set to zero until t = 1 second.

This indicates that the PV output is constant since the duty cycle remains constant at 0.5 until t = 0.4, after which the duty cycle slightly decreases to reduce the PV output until it is zero at t = 1 second. The temperature, fixed at 25°C, does not influence these variations.

Fig. 7(a) illustrates the CHBMLI output current under normal conditions, with the current reaching a range of 6 A, Figs. 7(b) and 7(c) display the output voltage of the CHBMLI, showing both the standard view and an expanded view, with a magnitude of 400V.

Fig. 7(d) presents the PV voltage over a period of 1 second, where it reaches a magnitude of 240V without any fault conditions. Fig. 7(e)

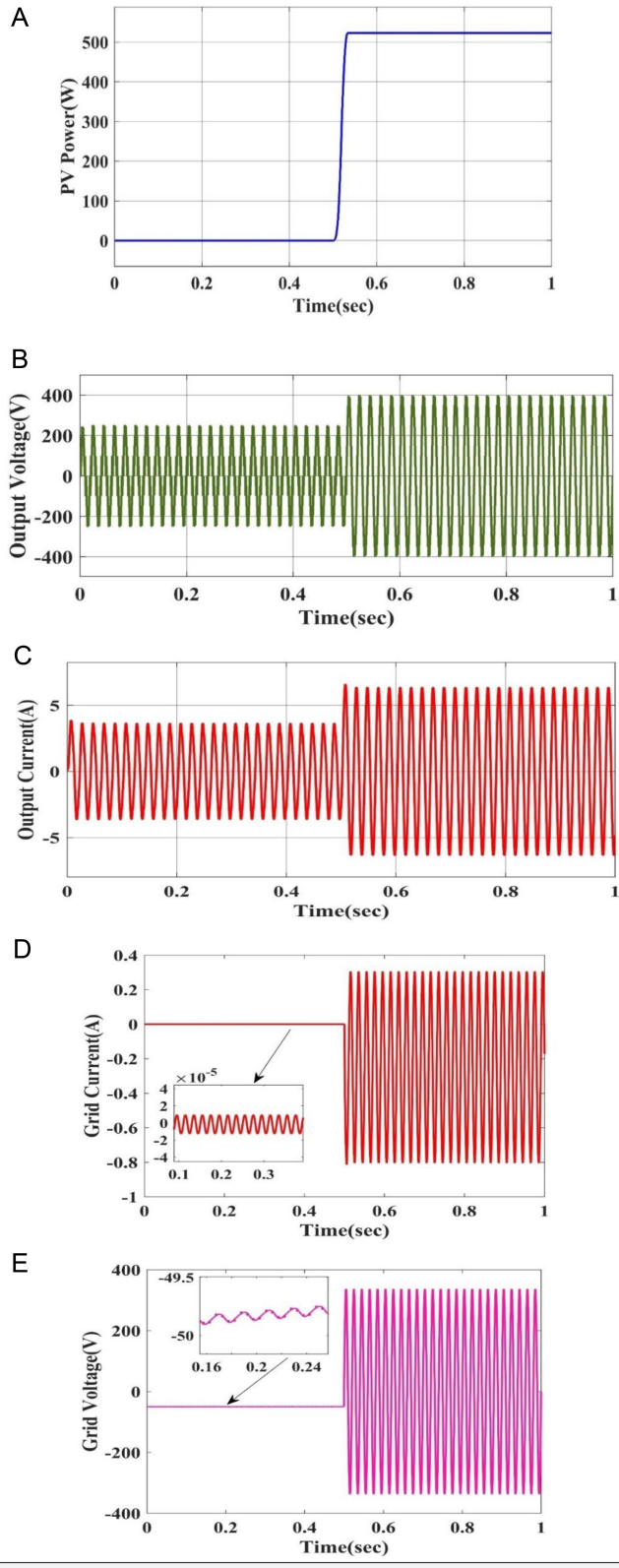

Fig. 9. Output response of CHBMLI with fault conditions: (a) PV power, (b) Output voltage, (c) Output current, (d) Grid current, and (e) Grid voltage.

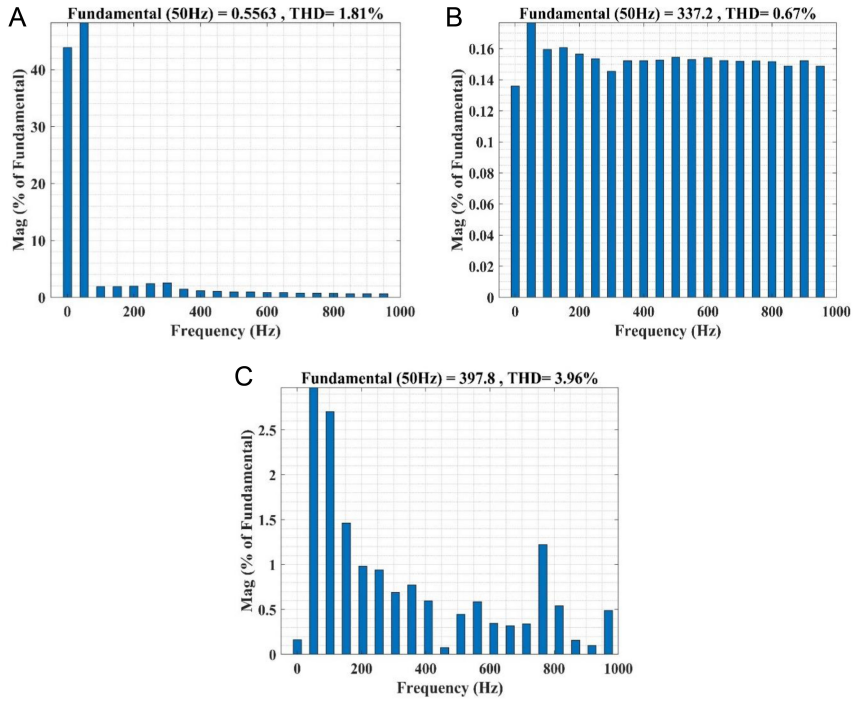

Fig. 10. THD analysis of (a) Grid voltage, (b) Grid current, and (c) 17-level CHBMLI voltage.

shows the PV current over the same 1-second period, initially rising rapidly to around 250 A before experiencing fluctuations and eventually dropping to zero. Lastly, Fig. 7(f) depicts the PV power (in Watts) over time, starting from zero, quickly increasing to approximately 700 W within the first 0.1 seconds, and then stabilizing with slight fluctuations. The rapid rise and eventual stabilization of PV current and power indicate effective system performance without fault disturbances.

Fig. 8(a) indicates the grid current over 1 second. The current oscillates between around −0.4 A and 0.4 A, showing an AC current flow. Fig. 8(b) indicates the grid voltage waveform over 1 second. The voltage has an AC signal pattern, although the amplitude is slightly lower than the anticipated ±400 V, which is likely due to system losses and filtering effects. Fig. 8(c) presents the grid voltage harmonics analysis. It is observed from Fig. 8(c), the amplitude is normalized, with the fundamental component expressed as a relative quantity rather than the absolute value of the voltage. According to IEEE 519 standards for harmonic analysis, the THD of 0.03% is determined as the ratio of harmonic components to the fundamental component.

Fig. 8(d) shows the harmonic spectrum investigation of the grid current using a proposed method. The fundamental frequency is 50 Hz with a magnitude of approximately 337.4 of the fundamental component. The harmonics for the grid current is 0.06 %. Fig. 8(e) represents the harmonic spectrum and harmonics for the output of a 17-level CHBMLI. The fundamental frequency here is 50 Hz with a magnitude of approximately 395.9% of the fundamental component. The THD is significantly lower at 2.35%, which suggests that the 17-level CHBMLI is effective in reducing harmonics compared to the grid voltage and current.

B. Case 2

The grid-connected PV system for linear load with fault conditions is displayed in this section under continuous radiation of 1000 W/m^2. Phase-phase faults are taken into consideration.

The output response of the CHBMLI under fault situations is shown in Fig. 9. In Fig. 9(a), the PV power response at the 1-second mark reaches 520 W. Fig. 9(b) shows that during the fault, up to 0.5 seconds, the output voltage decreases to 210 V, then rises to a voltage level of 400 V. The output current at one second is shown in Fig. 9(c), where it fluctuates between −4.8 A and +4.8 A for 0.5 seconds. The current rises to a range of −5.5 A to +5.5 A after 0.5 seconds. In Figs. 9(d) and 9(e), grid current and voltage are close to zero from 0 to 0.5 seconds, showing no power transfer. Both signals increase after 0.5 seconds, with current oscillating between −0.8 A and +0.3 A, and voltage from −300 V to +300 V, showing system activation.

Thus, it reveals that under fault conditions, the CHBMLI experiences fluctuations in output power, voltage, and current, with PV power peaking at 520 W and voltage initially dropping to 210 V before recovering to 400 V. Additionally, both grid current and voltage remain near zero for the first 0.5 seconds, subsequently increasing to ranges of −0.8 A to +0.3 A and −300 V to +300 V, indicating a delayed recovery after the fault.

Fig. 10 (a-c) illustrates the harmonic spectrum and THD of various system components. In Fig. 10(a), the fundamental frequency is 50 Hz with a magnitude of approximately 0.5563, and the THD is relatively low at 1.81%. Fig. 10(b) shows the fundamental frequency at 50 Hz with a magnitude of about 337.2, and the THD is similarly low at 0.67%. Fig. 10(c) indicates a fundamental frequency of 50 Hz with a magnitude of approximately 397.8, with the THD significantly reduced

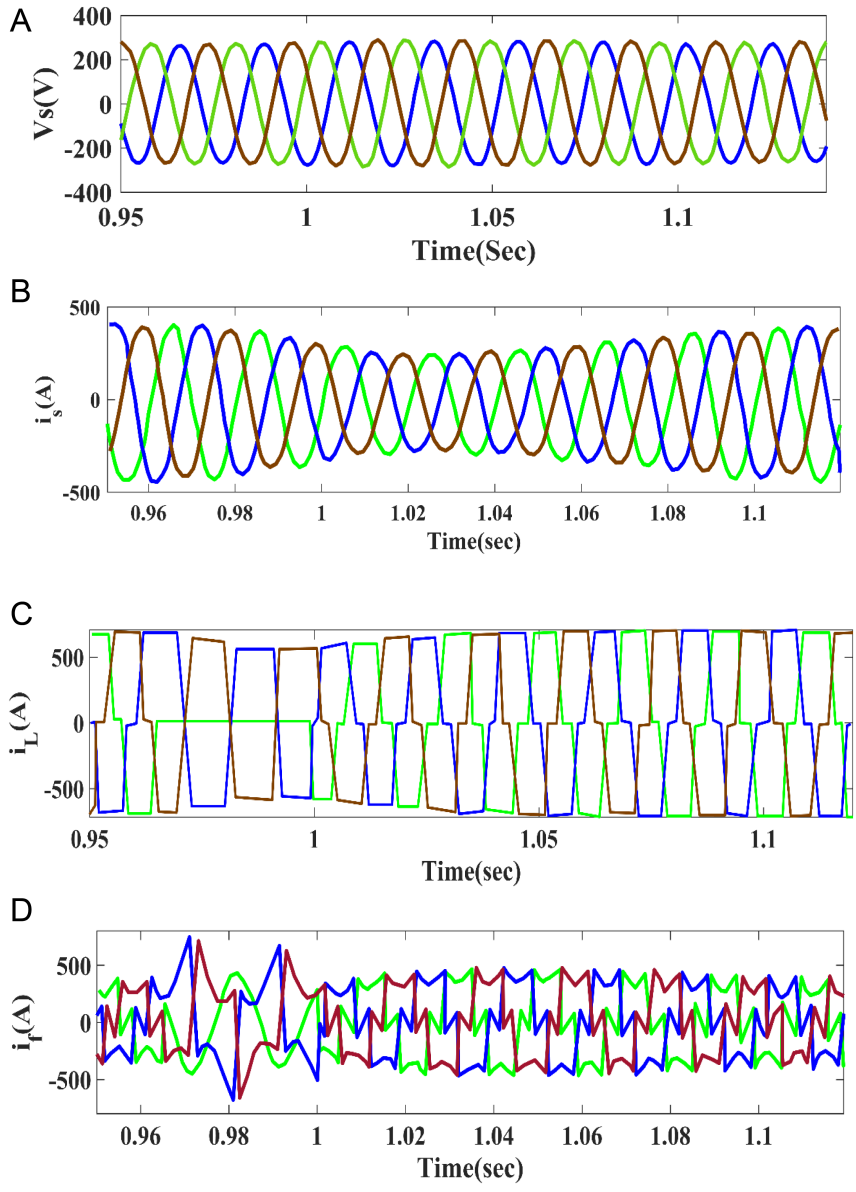

Fig. 11. Analysis of (a) source voltage, (b) source current, (c) load current, and (d) compensation current in case 3.

to 3.96%. This suggests that the 17-level CHBMLI is highly effective in minimizing harmonics compared to the grid voltage and current.

C. Case 3

The PV performance during imbalanced operation and non-linear load is shown in Fig. 11. The PV keeps balanced source currents without sacrificing power quality while one of the load's phases is cut off for a predetermined amount of time. Fig. 11(a) is a source voltage plot, while Fig. 11(b) shows the corresponding source current. The load current fluctuation at the time when phase-b is interrupted is depicted in Fig. 11(c), and currents of compensation generated by the PV are presented in Fig. 11(d).

D. Case 4

The source voltage and source current waveforms for the three-phase non-linear load that the source is feeding are displayed in Fig. 12. Fig. 12 (a) displays the source voltages, while Fig. 12 (b) displays the source current waveforms. The load currents are displayed in Fig. 12(c), and Fig. 12(d) shows the corresponding PV currents. Depending on the PV output, the PV contributes a portion of the active power and meets the load's reactive power and harmonic requirements.

Fig. 13(a) shows the harmonic spectrum of the non-linear and unbalanced load current. Fig. 13(b) shows that even with the non-linear load, the source currents remain balanced and harmonic-free. The PV reduces the source current THD to 1.65% by dispersing reactive and harmonic components to meet load demands.

Table IV summarizes the simulation results under different levels of solar irradiance. For irradiance levels of 1000, 500, and 100 W/m^2, the maximum outputs are as follows: at 1000 W/m^2, 600 W of power, 4.95

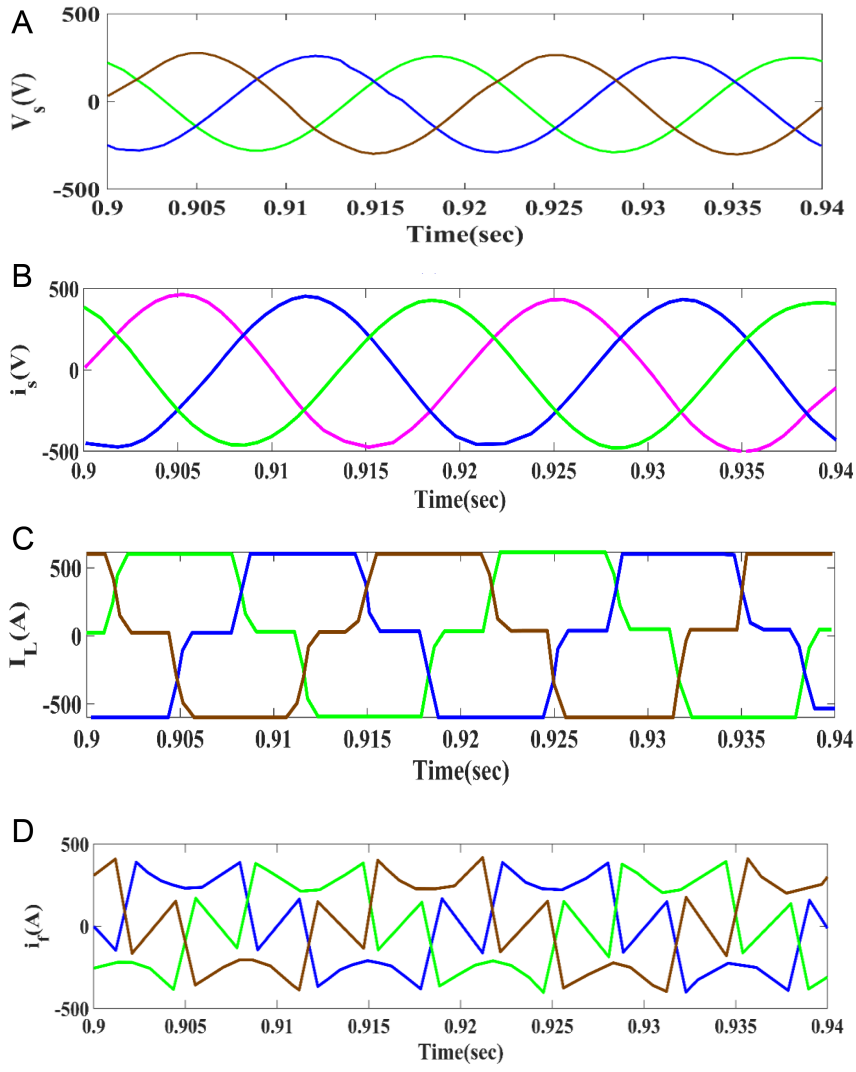

Fig. 12. Analysis of (a) source voltage, (b) source current, (c) load current, and (d) compensation current in case 4.

A of current, 140 V of voltage, and a duty cycle of 0.5; at 500 W/m^2, 558.2 W of power, 2.37 A of current, 115.2 V of voltage, and a duty cycle of 0.35; and at 100 W/m^2, 480.2 W of power, 0.431 A of current, 105.8 V of voltage, and a duty cycle of 0.002. Thus, it shows that as solar irradiance decreases from 1000 to 100 W/m^2, the maximum power, current, and voltage output also decline, with significant reductions in duty cycle values. Specifically, power decreases from 600 W at 1000 W/m^2 to 480.2 W at 100 W/m^2, indicating the system's performance is highly dependent on solar irradiance levels.

Important parameters such as the number of switches, diodes, DC sources, drive board circuits, Fundamental Component Compression (FCC), Total Switching Voltage (TSV), number of DC link capacitors, THD, and Crest Factor (CF) are listed in Table V, which provides a comparative overview of various multilevel inverter topologies from various sources. The suggested topology contains the minimum number of diodes (12) and DC-link capacitors (0) compared to the topologies under comparison. The proposed MLI topology achieves a THD of 2.35% and a CF of 3.1, which are among the better performances. The TSV for the proposed topology is 17, indicating a relatively low voltage stress on the components. Overall, the proposed MLI topology exhibits favorable characteristics across the evaluated metrics compared to other topologies.

IV. CONCLUSION

As a crucial part of the hybrid approach, this research presents the cascaded H-bridge multilevel inverter, which uses MPPT control to maximize PV system efficiency in stable solar circumstances. MATLAB simulations are used to improve PQ and filter harmonics in solar PV systems. The research also examines the dynamic performance of a grid-connected PV system with constant irradiation, analyzing both PV power output and total harmonic distortion. The system's response to load disturbances, including scenarios with and without faults—particularly line-to-line faults—is evaluated. The use of the 17-level CHBMLI is highly effective in increasing the PV power to 700 W. Future research could focus on optimizing the inverter design for varying solar irradiance and load profiles, developing

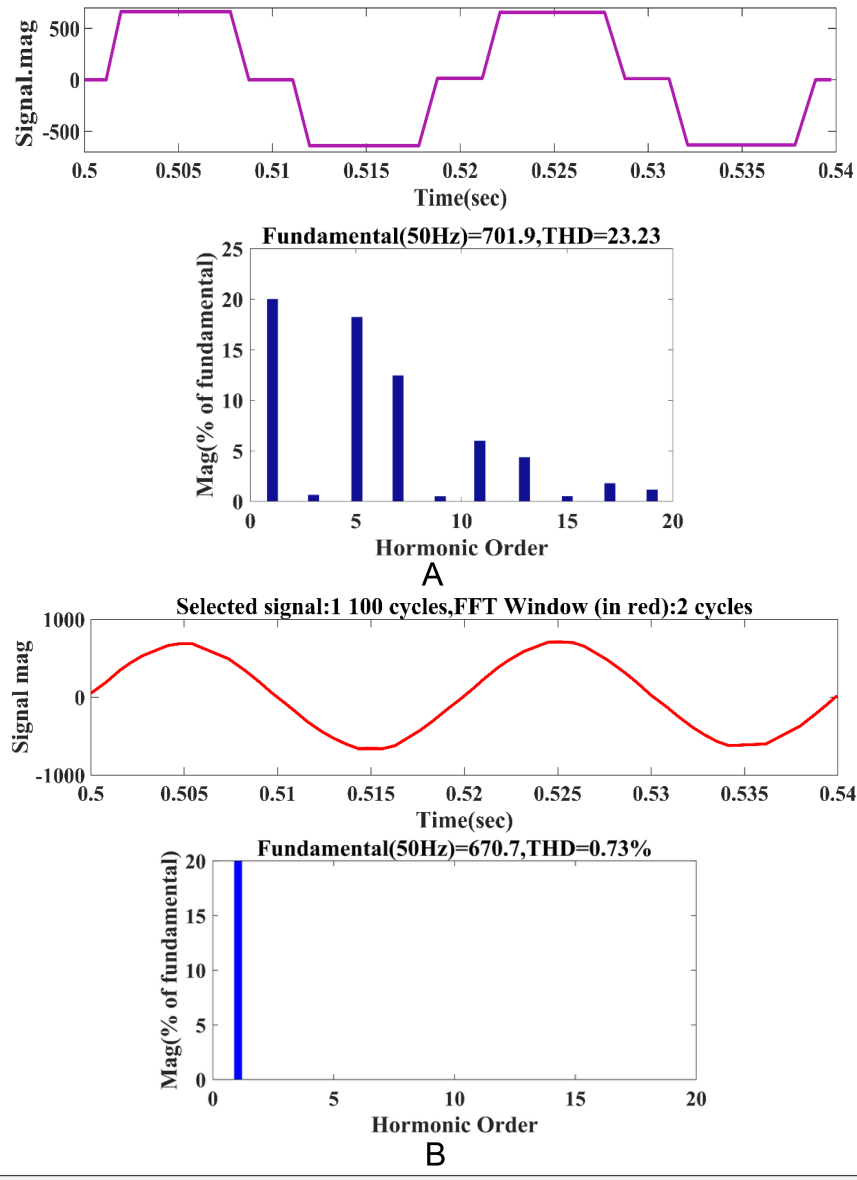

Fig. 13. Analysis of (a) harmonic spectrum of unbalanced and non-linear load current, and (b) balanced and harmonic-free source currents.

TABLE IV. SIMULATION PV OUTPUTS WITH SOLAR IRRADIATIONS

Solar Irradiations W/m²	Power Max (W)	Current Max (A)	Voltage Max (V)	Duty Cycle
1000	700	4.95	140	0.5
900	594.5	4.43	135.2	0.45
800	580.3	3.97	126.5	0.42
700	575.2	3.405	120.3	0.41
600	560	2.82	118.5	0.38
500	558.2	2.37	115.2	0.35
400	530.2	1.85	112.1	0.31
300	525.1	1.36	110.5	0.25
200	510.5	0.852	108.2	0.18
100	480.2	0.431	105.8	0.002

advanced control algorithms for dynamic fault detection and isolation, integrating energy storage systems to further enhance PQ and resilience, and conducting real-time hardware testing under diverse conditions to validate and refine these techniques. Under different solar irradiance conditions, the performance of the system is also adjusted. At 1000 W/m^2, it delivers 600 W of power, 4.95 A of current, 140 V of voltage, and a duty cycle of 0.5. Under a reduction in irradiance to 500 W/m^2, the power is 558.2 W, the current is 2.37 A, the voltage is 115.2 V, and the duty cycle is 0.35. At the lowest irradiance level of 100 W/m^2, power is reduced to 480.2 W, current to 0.431 A, voltage to 105.8 V, and duty cycle to 0.002, indicating the reliance of the system on solar supply. The selected multilevel inverter configuration demonstrates robust operation with a very low THD of 2.35%, a CF of 3.1, and a TSV of 17, utilizing a mere 12 diodes and no DC-link capacitors. Moreover, the system efficiently compensates for harmonics and reactive power, lowering the source current THD to 1.65%, and providing balanced, distortion-free currents even in

TABLE V. COMPARISON OF 17 LEVEL MLI TOPOLOGIES

Citation	Ns	No of Diodes	No of dc-Link Capacitors	DC Source	Drive Board Circuits	FCC	TSV	THD	CF (0.5)
[25]	20	20	4	2	20	3.88	–	–	–
[26]	16	16	4	4	14	3.17	11	–	3.5
[27]	24	24	4	2	24	4.48	–	–	–
[28]	10	10	4	2	20	3.88	–	–	–
[29]	14	20	4	8	14	3.52	22	–	4.17
[30]	10	12	0	2	10	2	40	–	5.18
[31]	10	10	0	4	10	2	36	7.1	4.94
[32]	20	20	0	8	20	4	36	3.7	5.05
[33]	14	16	4	4	14	3.05	11	4.23	3.38
Proposed	12	12	0	3	10	2.02	17	2.35	3.1

nonlinear load conditions. In the future, the research will be further extended by simulating realistic solar panel characteristics to verify the performance of the system under real-world interconnection conditions.

Data Availability Statement: The data that support the findings of this study are available on request from the corresponding author.

Peer-review: Externally peer-reviewed.

Author Contributions: Concept – V.S.P.; – Design – V.S.P.; – Supervision – P.J.G.; – Resources – P.J.G.; – Materials – V.S.P.; – Data Collection and/or Processing – V.S.P.; – Analysis and/or Interpretation – V.S.P.; – Literature Search – V.S.P.; – Writing Manuscript – V.S.P.; Critical Review – P.J.G.

Declaration of Interests: The author has no conflict of interest to declare.

Funding: The authors declared that this study has received no financial support.

REFERENCES

1. N. Mukundan, and P. Jayaprakash, "Realization of cascaded H-bridge multilevel inverter based grid integrated solar energy system with band stop generalized integral control," *IEEE Trans. Ind. Appl.*, vol. 57, no. 1, pp. 764–773, 2020. [CrossRef]
2. A. A. Stonier, S. Murugesan, R. Samikannu, S. K. Venkatachary, S. S. Kumar, and P. Arumugam, "Power quality improvement in solar fed cascaded multilevel inverter with output voltage regulation techniques," *IEEE Access*, vol. 8, pp. 178360–178371, 2020. [CrossRef]
3. S. Adak, and H. Cangi, "The quality problems at low irradiance in the grid-connected photovoltaic systems," *Electr. Eng.*, vol. 106, no. 5, pp. 6185–6197, 2024. [CrossRef]
4. E. J. Mol, and M. M. Linda, "Higrid connected DFIG-based wind turbine and solar PV energy system using fuzzy logic controller," *Solid State Technol.*, vol. 64, no. 2, pp. 2342–2356, 2021.
5. A. Amir, A. Amir, J. Selvaraj, and N. Abd Rahim, "Grid-connected photovoltaic system employing a single-phase T-type cascaded H-bridge inverter," *Sol. Energy*, vol. 199, pp. 645–656, 2020. [CrossRef]
6. P. R. Bana, K. P. Panda, and G. Panda, "Power Quality Performance Evaluation of multilevel inverter with reduced switching devices and minimum standing voltage," *IEEE Trans. Ind. Inform.*, vol. 16, no. 8, pp. 5009–5022, 2020. [CrossRef]
7. E. Jessy Mol, and M. Mary Linda, "Integration of wind and PV systems using genetic-assisted artificial neural network," *Intell. Autom. Soft Comput.*, vol. 35, no. 2, pp. 1471–1489, 2023. [CrossRef]
8. J. Jaya, and M. M. Linda, "A new-fangled approach for optimal placement of FACTS controllers in a hybridized system," *Electr. Power Compon. Syst.*, pp. 1–17, 2024. [CrossRef]
9. A. Sahli, F. Krim, A. Laib, and B. Talbi, "Energy Management and Power Quality Enhancement in grid-tied single-phase PV system using modified PUC converter," *IET Renew. Power Gener.*, vol. 13, no. 14, pp. 2512–2521, 2019. [CrossRef]
10. J. Wang, K. Sun, H. Wu, J. Zhu, Y. Xing, and Y. Li, "Hybrid connected unified power quality conditioner integrating distributed generation with reduced power capacity and enhanced conversion efficiency," *IEEE Trans. Ind. Electron.*, vol. 68, no. 12, pp. 12340–12352, 2021. [CrossRef]
11. C. R. Rajesh, P. Meenalochini, S. K. Kannaiah, and A. Bindu, "A hybrid control topology for cascaded H-bridge multilevel inverter to improve the power quality of smart grid connected system: NBO-RERNN approach," *Expert Syst. Appl.*, vol. 238, p. 122054, 2024. [CrossRef]
12. S. K. Yadav, N. Mishra, and B. Singh, "An improved multicarrier PWM technique for harmonic reduction in cascaded H-bridge based Solar Photovoltaic System," *IEEE Trans. Ind. Inform.*, vol. 20, no. 7, pp. 9205–9214, 2024. [CrossRef]
13. G. Anusha, K. Arora, H. Sharma, S. P. Thota, G. P. Joshi, and W. Cho, "Control strategies of 15-level modified cascaded H-bridge MLI with solar PV and Energy Storage System," *Energy Rep.*, vol. 12, pp. 2–26, 2024. [CrossRef]
14. P. K. Chamarthi, U. R. Muduli, M. S. E. Moursi, A. Al-Durra, A. S. Al-Sumaiti, and K. A. Hosani, "Improved PWM approach for cascaded five-level NPC H-bridge configurations in multilevel inverter," *IEEE Trans. Ind. Appl.*, vol. 60, No. 5, pp. 7048–7060, 2024. [CrossRef]
15. R. K. Jain, B. V. Reddy, and G. H. K. Varma, "Robust and efficient control strategy for single-phase two-stage PV grid-tied system with improved power quality," *Renew. Energy Focus*, vol. 48, p. 100524, 2024. [CrossRef]
16. D. A. Prasad, G. Muralikrishnan, C. Navaneethan, and S. Meenatchi, "A novel modified switched capacitor multilevel inverter using SARC-DQRLC controlling mechanisms for grid systems," *Int. J. Hydrog. Energy*, vol. 77, pp. 40–53, 2024. [CrossRef]
17. S. Ranjan Das *et al.*, "Fuzzy controller designed-based multilevel inverter for power quality enhancement," *IEEE Trans. Con. Electron.*, vol. 70, no. 2, pp. 4839–4847, 2024. [CrossRef]
18. R. Mohanty *et al.*, "Lower output voltage harmonics with optimum switching angles of single PV-source based reduced switch multilevel inverter using BWO algorithm," *IEEE Access*, vol. 12, pp. 5054–5065, 2024. [CrossRef]
19. A. Govind, K. Jayaswal, V. K. Tayal, and P. Kumar, "Simulation and real time implementation of shunt active power filter for power quality enhancement using adaptive neural network topology," *Electr. Power Syst. Res.*, vol. 228, p. 110042, 2024. [CrossRef]
20. P. Bansal, S. Dixit, S. Gupta, M. A. Alotaibi, H. Malik, and F. P. G. Márquez, "A robust modified notch filter based SOGI-PLL approach to control

multilevel inverter under distorted grid," *Ain Shams Eng. J.*, vol. 15, no. 5, p. 102675, 2024. [CrossRef]
21. B. Abdollahzadeh *et al.*, "Puma Optimizer (PO): A novel metaheuristic optimization algorithm and its application in machine learning," *Clust. Comput.*, pp. 1–49, 2024. [CrossRef]
22. M. Wang, L. Yan, J. Jia, J. Lai, H. Zhou, and B. Yu, "DE-MHAIPs: Identification of SARS-COV-2 phosphorylation sites based on differential evolution multi-feature learning and multi-head attention mechanism," *Comput. Biol. Med.*, vol. 160, p. 106935, 2023. [CrossRef]
23. P. Dileep *et al.*, "An automatic heart disease prediction using Cluster-based bi-directional LSTM (C-bilstm) algorithm," *Neural Comput. Appl.*, vol. 35, no. 10, pp. 7253–7266, 2023. [CrossRef]
24. V. Kumar, R. Kumar, and R. K. Jarial, "Power Quality Enhancement of dual stage three phase grid integrated SPV system using sequential neural network-based algorithm," *Electr. Power Syst. Res.*, vol. 230, p. 110246, 2024. [CrossRef]
25. A. Tirupathi, K. Annamalai, and S. Veeramraju Tirumala, "A new hybrid flying capacitor–based single-phase nine-level inverter," *Int. Trans. Electr. Energy Syst.*, vol. 29, no. 12, 2019. [CrossRef]
26. P. Bhatnagar, R. Agrawal, and K. K. Gupta, "Reduced device count version of single-stage switched-capacitor module for cascaded multilevel inverters," *IET Power Electron.*, vol. 12, no. 5, pp. 1079–1086, 2019. [CrossRef]
27. S. S. Lee, "Single-stage switched-capacitor module (s3cm) topology for cascaded multilevel inverter," *IEEE Trans. Power Electron.*, vol. 33, no. 10, pp. 8204–8207, 2018. [CrossRef]
28. S. S. Lee, C. S. Lim, and K.-B. Lee, "Novel active-neutral-point-clamped inverters with improved voltage-boosting capability," *IEEE Trans. Power Electron.*, vol. 35, no. 6, pp. 5978–5986, 2020. [CrossRef]
29. E. Samadaei, A. Sheikholeslami, S. A. Gholamian, and J. Adabi, "A square T-type (ST-type) module for asymmetrical multilevel inverters," *IEEE Trans. Power Electron.*, vol. 33, no. 2, pp. 987–996, 2018. [CrossRef]
30. R. Shalchi Alishah, S. H. Hosseini, E. Babaei, M. Sabahi, and G. B. Gharehpetian, "New high step-up multilevel converter topology with self-voltage balancing ability and its optimization analysis," *IEEE Trans. Ind. Electron.*, vol. 64, no. 9, pp. 7060–7070, 2017. [CrossRef]
31. J. Sathik Mohamed Ali *et al.*, "A new generalized multilevel converter topology based on cascaded connection of Basic Units," *IEEE J. Emerg. Sel. Top. Power Electron.*, vol. 7, no. 4, pp. 2498–2512, 2019. [CrossRef]
32. M. N. Hamidi, D. Ishak, M. A. A. M. Zainuri, and C. A. Ooi, "Multilevel inverter with improved basic unit structure for symmetric and asymmetric source configuration," *IET Power Electron.*, vol. 13, no. 7, pp. 1445–1455, 2020. [CrossRef]
33. C. Dhanamjayulu, D. Prasad, S. Padmanaban, P. K. Maroti, J. B. Holm-Nielsen, and F. Blaabjerg, "Design and implementation of seventeen level inverter with reduced components," *IEEE Access*, vol. 9, pp. 16746–16760, 2021. [CrossRef]
34. P. K. Chamarthi, V. Agarwal, and A. Al-Durra, "A new 1-ϕ, seventeen level inverter topology with less number of power devices for renewable energy application," *Front. Energy Res.*, vol. 8, p. 131, 2020. [CrossRef]

Mr. Vijay S. Pawar received his B.E. degree in Electrical Engineering from SSGMCE Shegaon in 1994 and his M.E. degree in Electrical Power System in 2001 from SSGMCE Shegaon. He is working as an Associate Professor at SSBT's COET Bambhori Jalgaon. He is pursuing a Ph.D. from Government Engineering College Jalgaon and from Kavyitri Bahinabai Chaudhari North Maharashtra University, Jalgaon. His research area is Power Quality in Grid-Connected Photovoltaic Systems.

Dr. Prashant J. Gaidhane received his BE degree in Instrumentation Engineering from SGGSCE&T Nanded, India, in 1998, his M. Tech degree in Instrumentation in 2009 from the Indian Institute of Science (IISc) Bangalore, India. He is working as an Associate Professor at Government College of Engineering, Jalgaon. He has completed his Ph.D. in Electronics and Communication Engineering Department at IIT Roorkee. His research area is evolutionary algorithms and their applications in Control System Design.